

pubs.acs.org/JPCL Letter

Synthesis and Optical Properties of Mn²⁺-Doped Amino Lead Halide Molecular Clusters Assisted by Chloride Ion

Li Liu, Keliang Pan,* Ke Xu, Xitian Peng, and Jin Z. Zhang*



Cite This: J. Phys. Chem. Lett. 2021, 12, 7497-7503



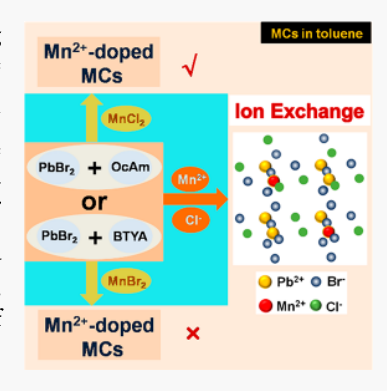
Read Online

ACCESS I

Metrics & More

Article Recommendations

ABSTRACT: Mn²⁺-doped amino lead halide molecular clusters (MCs) are synthesized using amine (e.g., n-octylamine, or butylamine) as passivating ligand and MnX₂ (X = Cl or Br) as the Mn²⁺ doping source at room temperature. Their optical properties are investigated with UV—visible absorption, photoluminescence (PL), and PL excitation spectroscopy. The Mn²⁺ precursor plays a vital role in the synthesis of Mn²⁺-doped MCs. MnCl₂ seems to facilitate the incorporation of Mn. The MnCl₂ doping causes electronic absorption blue shift and leads to a spin-forbidden ${}^4T_1 \rightarrow {}^6A_1$ Mn d-electron emission. With the help of time-resolved PL, Fourier transform infrared, and electron paramagnetic resonance results, a model is proposed to explain the formation mechanism. We suggest that Mn²⁺ doping replaces Pb²⁺ is assisted by Cl⁻ ions that replace Br⁻ ions. This study demonstrates the possibility of doping MCs and has important implications in gaining new fundamental insight into the growth mechanisms of perovskite nanostructures.



S emiconductor perovskite nanocrystals (PNCs) with a general formula ABX_3 , where A is a monovalent organic or inorganic cation (e.g., methylammonium (MA), formamidinium (FA) and Cs⁺), B is a metal cation (e.g., Pb²⁺ and Sn²⁺), and X is a halide anion (I⁻, Br⁻ or Cl⁻), are promising materials for a diverse range of applications such as lightemitting diodes (LEDs), solar cells, and photovoltaic (PV). However, because of the large surface-to-volume (S/V) ratio, the properties of such PNCs are heavily influenced by the structural and electronic character of the surface. Better control of the synthesis of PNCs and their surface chemistry is the key to achieving the above-mentioned properties and applications.

Recently, in our effort to understand the growth mechanism of PNCs⁷ and related magic sized clusters (MSCs),⁸ a new species named amino lead halide molecular clusters (MCs) was discovered.9 Compared with PNCs, MSCs and MCs are single sized and/or very narrow size distributed particles that are smaller and more uniform in size and shape. MSCs and MCs have bluer and sharper absorption and emission bands that are suitable for fundamental studies as well as emerging applications such as blue light emitters. Compared with PNCs or MSCs, MCs do not have the full perovskite composition since the normal A component was not present. The MCs are less ordered and do not have the perovskite crystal structure, and they are molecule-like. 10 Importantly, there is an equilibrium existing between MSCs and MCs. MSCs are converted spontaneously over time into MCs, and MCs can revert back to MSCs under the right experimental conditions. MCs can be viewed as important precursors in the formation of MSCs or PNCs. 11,12 Their unique characteristics, including small and supposedly single size as well as relatively strong photoluminescence (PL), make them intriguing for fundamental research and potentially useful for photonics applications such as blue single photon emitters.

Doping is a useful approach to altering electronic, optical, and magnetic properties of materials. 15 For example, extensive research has been conducted on Mn²⁺ doping of PNCs^{16–18} in which the Mn²⁺ dopant has characteristic PL around 580 nm, with a PL lifetime around 1.0 ms, of interest for light emission ^{19,20} and energy conversion. ²¹ We have previously shown that Mn²⁺ can be doped into perovskite MSCs.²² In this work, we demonstrate the first successful synthesis of Mn²⁺doped amino lead bromide MCs using amine (e.g., noctylamine (OcAm) or butylamine (BTYA)) as the only ligand together with MnCl₂ as the Mn²⁺ source at room temperature. We further determined the influence of the dopant precursor and doping concentration on the optical properties of the Mn²⁺-doped MCs. The Cl⁻ ion in the MnCl₂ precursor seems to play an important role in the doping of Mn²⁺, in a codoping manner, which is attributed to the similarity in bond energy between Mn-Cl and Pb-Cl.²³ With increasing concentration of MnCl₂, the absorption band blue shifts and a broad PL band peaked around 590 nm appears. A

Received: July 12, 2021 Accepted: July 30, 2021 Published: August 3, 2021





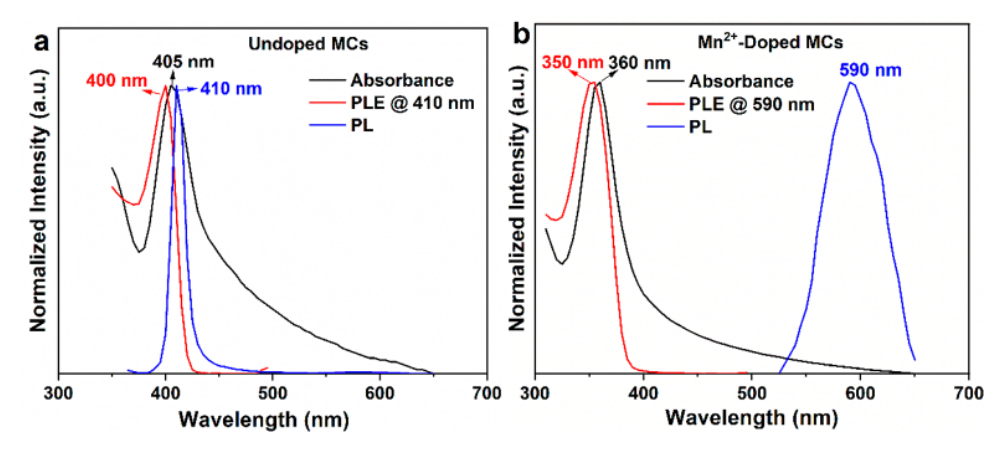


Figure 1. Optical properties of undoped and Mn^{2+} -doped MCs. UV-vis absorption (black), PL (blue), and PLE (red) spectra of (a) undoped and (b) Mn^{2+} -doped MCs.

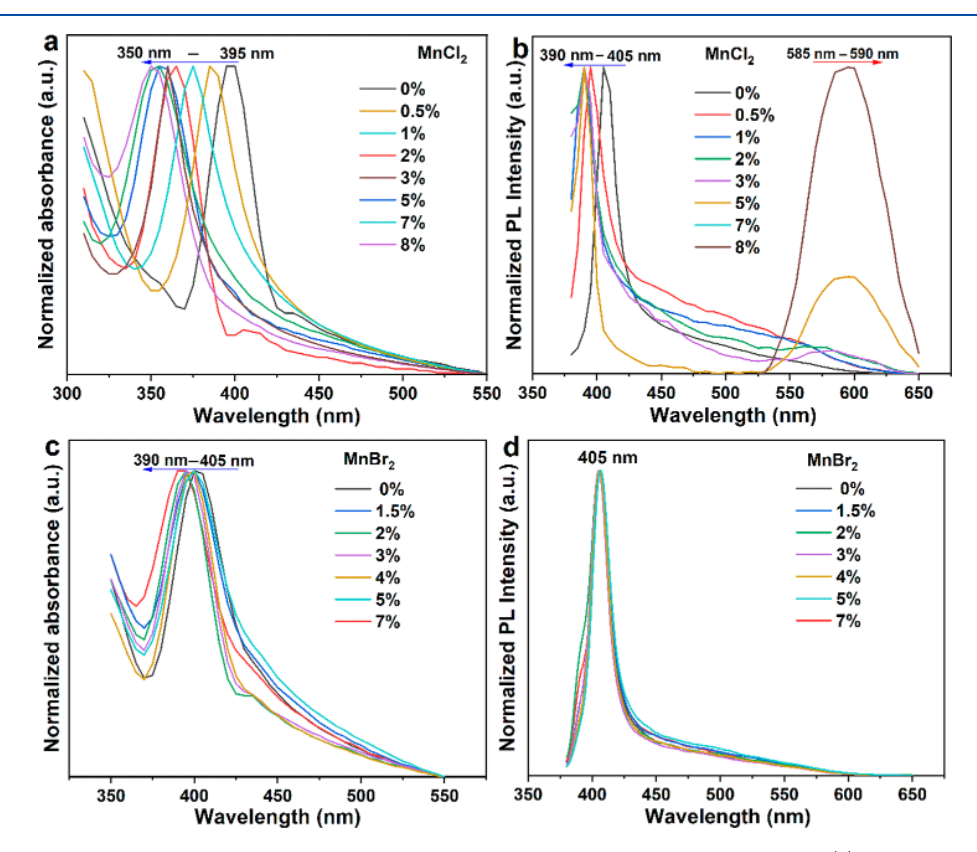


Figure 2. Dependence of PbBr₂—OcAm MCs optical properties on different doping precursor concentration. (a) Normalized absorption and (b) PL spectra of MCs of varying MnCl₂ doping concentration. (c) Normalized absorption and (d) PL spectra of MCs of varying MnBr₂ doping concentration.

combination of PL excitation (PLE), electron paramagnetic resonance (EPR), and time-resolved PL (TRPL) results confirms the successful doping of Mn²⁺.

The optical properties of Mn²⁺-doped and undoped PbBr₂—OcAm solutions samples are shown in Figure 1. For the undoped PbBr₂—OcAm sample, the UV—vis absorption spectrum exhibits a strong and sharp electronic absorption band peak at 405 nm, whereas the PL spectrum has an emission band peak at 410 nm. We attributed these absorption and emission bands to MCs based on our previous work. The PLE spectra collected at 410 nm emission shows a peak near 400 nm that is close to the electronic absorption peak. This

indicates that the 410 nm emission originates from electronic excitation of the host MCs. 24,25

The $\rm Mn^{2+}$ -doped PbBr $_2$ –OcAm sample with 8% of Mn doping (at. %) introduced shows an absorption band that peaked at 360 nm and a PL band centered on 590 nm. The emission peak at 590 nm is characteristic of and thereby attributed to a Mn d–d spin-forbidden $^4\rm T_1 \rightarrow ^6\rm A_1$ transition. 26 This indicates successful doping of Mn $^{2+}$ into the host MCs. Importantly, for the Mn $^{2+}$ -doped PbBr $_2$ –OcAm sample, the PLE spectra collected at 590 nm emission shows a band peaked around 350 nm, which is very close to the electronic absorption band of the doped MCs. This reveals that the Mn $^{2+}$

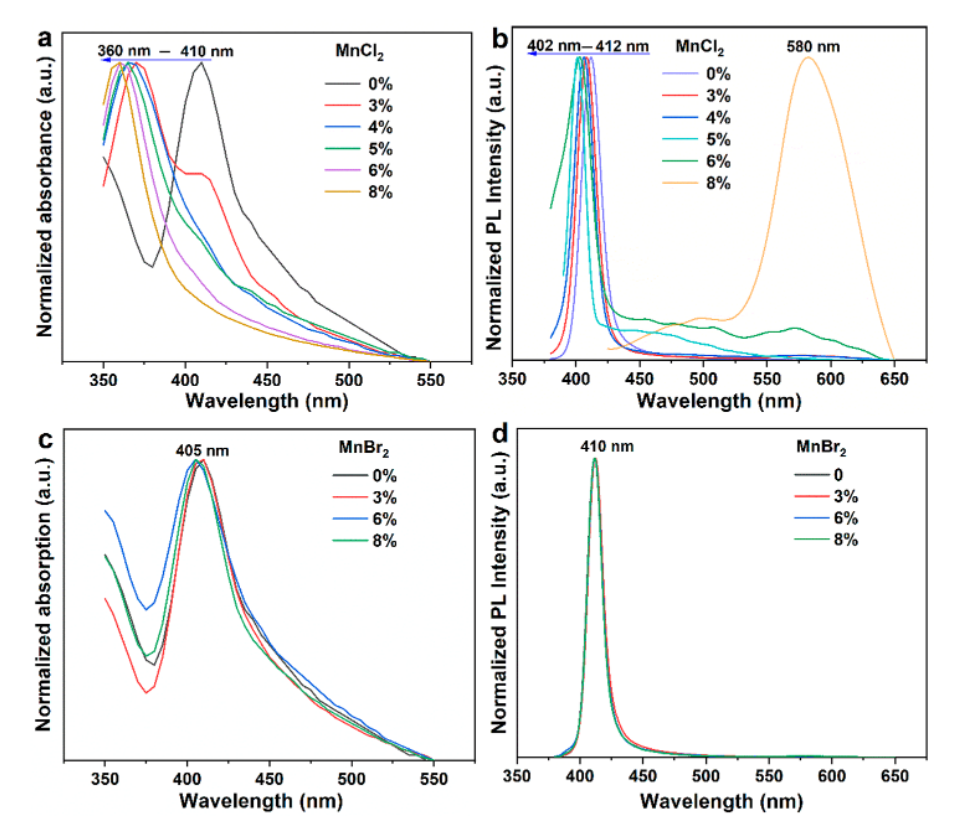


Figure 3. Dependence of PbBr₂–BTYA MCs optical properties on different doping precursor concentration. (a) Normalized absorption and (b) PL spectra of MCs of varying MnCl₂ doping concentration. (c) Normalized absorption and (d) PL spectra of MCs of varying MnBr₂ doping concentration.

emission is due to electronic absorption of the doped MCs. The PLE spectrum confirms that the 590 nm from $\rm Mn^{2+}$ originated from the electronic absorption of the doped MCs and successful doping of $\rm Mn^{2+}$ into the MCs.

To better understand the nature of Mn²⁺ doping, the absorption and PL spectra of PbBr2-OcAm MCs prepared with different amount of Mn precursors are shown in Figure 2. With increasing amount of $\bar{M}n^{2+}$, the electronic absorption peak systematically blue shifts from 395 to 350 nm. This is somewhat unexpected because usually doping does not affect noticeably the absorption spectrum. 21,27 The blue-shifted electronic absorption band for the doped samples compared with the undoped sample suggested that Mn²⁺-doping fundamentally altered the energy gap between the ground state and the first excited electronic state of the doped MCs. The dopant has a significant effect on the electronic structure of the host MCs. Another possible explanation is that the doped MCs are smaller in size than the undoped ones and have more localized electronic wave functions, which is essentially quantum confinement. Furthermore, since MnCl₂ is used as the doping precursor, there is possibly anion exchange between Cl and Br, which would increase the excited state-ground state energy gap of the host MCs and also lead to a blue shift in absorption. 22,28 Meanwhile, for the Mndoped samples, the host emission at 405 nm first blue shifts and then disappears at a high doping level, while the Mn d-d emission was observed and slightly shifts from 585 to 590 nm. At this point, it is not yet clear whether the blue shift of the host electronic absorption peak is due to Cl/Br exchange, decreased MC size, or influence of the Mn dopant, which

requires further study in the future, as explained later. The decreased host PL intensity is associated with increased Mn PL intensity when the dopant level was increased, and this can be explained by a higher percentage of MCs being doped with increasing dopant concentration. The results also seem to indicate the transfer of energy from the host MCs to the Mn dopant is highly efficient.

To determine if the above-mentioned blue-shifted spectra upon doping is due to Cl/Br exchange, MnBr $_2$ was studied as a precursor of Mn $^{2+}$ doping. As shown in Figure 2c,d, all samples show a sharp absorption band around 400 nm and a corresponding characteristic MCs emission near 405 nm. In this case, Mn $^{2+}$ doping has little effect on the optical properties of MCs, and there is no Mn $^{2+4}$ T $_1 \rightarrow {}^6$ A $_1$ emission observed. It appears that under the current experimental conditions studied, it is not possible to dope the MCs using MnBr $_2$. This seems to suggest the Cl $^-$ ion seems to be playing an important role in the Mn doping, possibly similar to a codoping scheme. $^{30-32}$

To determine the generality of the demonstrated doping approach of the MCs, we studied the doping process of the MCs using a different amine ligand, BTYA, instead of OcAm. The UV—vis and PL spectra of PbBr₂—BTYA MCs with different amounts of MnCl₂ introduced are shown in Figure 3. For PbBr₂—BTYA MCs without doping, a strong absorption band peak at 410 nm is observed, along with a PL peak at 412 nm, as we reported previously. For doped PbBr₂—BTYA MCs, though Mn²⁺ was added to all the samples, the Mn²⁺ 590 nm d—d emission was only observed in the case of the high concentration of MnCl₂ but not MnBr₂. Specifically, as the

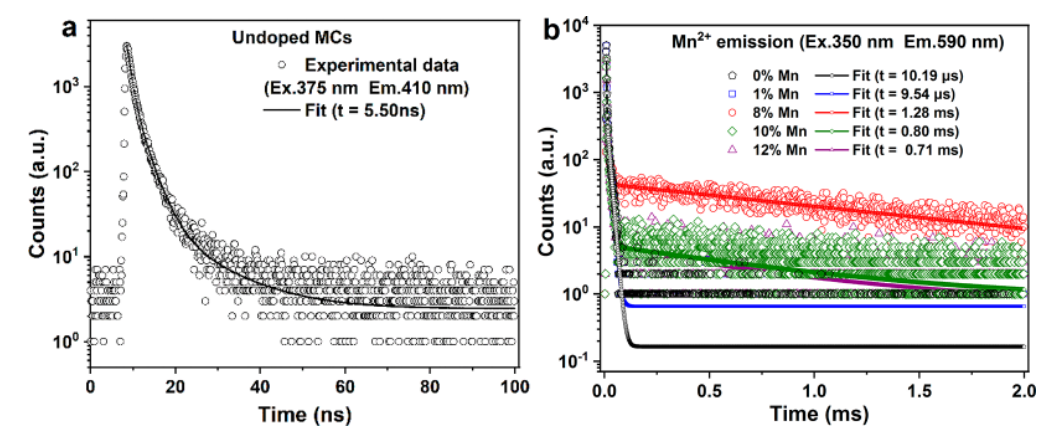


Figure 4. Normalized TRPL decay curves of (a) undoped MCs by exciting at 375 nm and monitoring the emission at 410 nm and (b) Mn^{2+} -doped MCs with different doping levels (0, 1, 8, 10, 12% at. %) by exciting at 350 nm and monitoring the emission at 590 nm. The symbols are experimental data, and solid lines are corresponding fits using an exponential decay function.

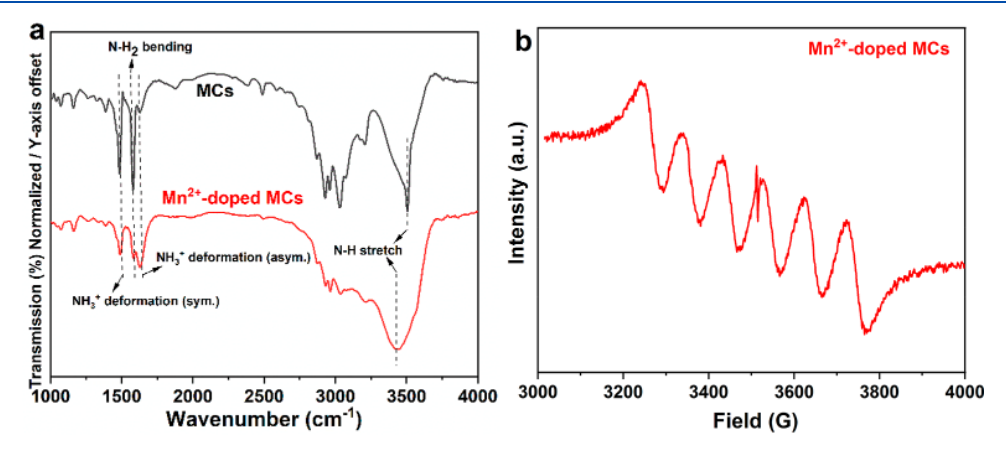


Figure 5. (a) FTIR spectra of Mn²⁺-doped and undoped MCs. (b) Room-temperature X-band EPR spectra of Mn²⁺-doped MCs.

MnCl₂ concentration increases, the absorption peak blue-shifted from 410 to 360 nm while the host PL peak blue-shifted from 412 to 402 nm and then disappeared at 8% of MnCl₂, where the dopant Mn d—d emission was appeared. At the same 8% concentration for MnBr₂, no Mn PL emission was observed. In this case, the host absorption peak and PL peak did not blue shift with increasing MnBr₂ concentration. The results show that the identity of the Mn²⁺ doping precursor plays a vital role in the synthesis of Mn²⁺-doped MCs.

When MnBr₂ precursor is used, no anion exchange is possible since there is no Cl⁻ introduced; further, the addition of Mn²⁺ alone to the MCs did not significantly change the optical characteristics of MCs, and there is no Mn²⁺ emission observed even at high Mn2+ concentration. At this point, we ruled out the previous hypothesis that Mn²⁺-addition affects the electronic structure of the host MCs, which leads to the blue shift in absorption. When MnCl₂ precursor is selected, a significant blue shift of the UV-vis absorption and a Mn PL emission was observed, indicating that the codoping with Clresults in Mn²⁺ internal doping.³³ A similar preference of Mn doping in cesium lead halide perovskite was also reported, 34,35 where no characteristic Mn²⁺ d-d emission in the product nanocrystals was observed when MnBr2 and manganese carboxylates were used.²³ They suggest that the success of using MnCl₂ as a precursor for doping can be attributed to the similarity in bond strength within the precursor and the

growing lattice (the bond dissociation energy of Mn–Cl, Pb–Cl, Mn–Br, and Pb–Br is 338, 301, 314, and 249 kJ/mol, respectively). ³⁶ In our approach, when Cl⁻ was introduced along with Mn²⁺, halide anion exchange likely occurs between Br⁻ and Cl⁻ in solution, leading to the formation of PbCl₂, which is conducive to the formation of doped MCs because the bond energy between Mn–Cl and Pb–Cl is similar.

To further confirm the Mn doping, the PL lifetimes of the undoped MCs and Mn²⁺-doped MCs samples were measured using TRPL spectroscopy. For the undoped MCs, the TRPL result was obtained by exciting at 375 nm and monitoring at 410 nm. The PL decay profiles can be fit to an exponential function with a lifetime of 5.50 ns (Figure 4a). For the Mn²⁺doped MCs, the TRPL result was obtained by exciting at 350 nm and monitoring at 590 nm. Interestingly, the lifetime of the Mn²⁺ emission seems to depend strongly on the Mn doping level. As shown in Figure 4b, at a lower Mn²⁺ concentration (0-1%), the lifetime slightly decreased from 10.19 to 9.54 μ s. At higher Mn^{2+} concentrations (8–12%), the lifetime decreased from 1.28 to 0.71 ms. Since the characteristic PL lifetime of Mn^{2+} emission is ~ 1.0 ms, this indicates that only relatively high Mn²⁺ concentration leads to doping. Low Mn²⁺ concentration does not lead to doping, but halogen ion exchange between Cl⁻ and Br⁻ can occur. The slight decrease in lifetime at even higher Mn²⁺ concentrations may be caused by Mn-Mn coupling that can quench the Mn PL.29

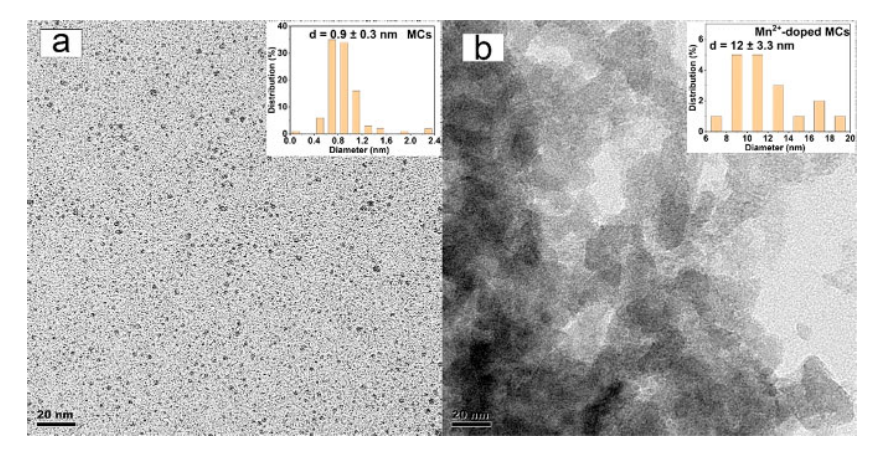


Figure 6. TEM image of (a) undoped and (b) Mn²⁺-doped MCs. Insets show particle size distribution histogram of undoped and Mn²⁺-doped MCs

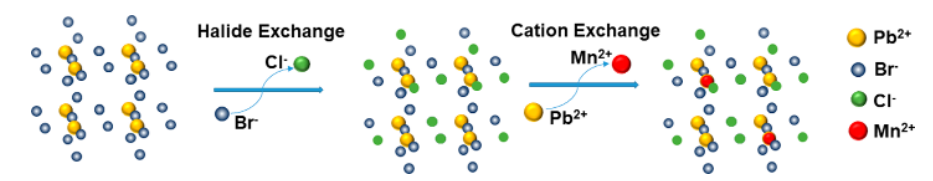


Figure 7. Schematic illustration of Mn²⁺-doped amino lead halide MCs.

Importantly, the TRPL data support successful doping of Mn into the MCs.

In addition, Fourier transform infrared (FTIR) spectra were taken for the Mn²⁺-doped and undoped MCs (Figure 5a). The characteristic bands at 1490 and 1625 cm⁻¹ are attributed to the symmetric and asymmetric deformation vibrations of the NH₃⁺ group, respectively. The NH₂ bending for free amine at around 1600 cm⁻¹ shifts to 1580 cm⁻¹, consistent with a shift to lower frequency when amine is bound to metals, indicating the presence of amine ligands on or near the surface of the MCs. Interestingly, the doping of Mn²⁺ causes the sharp peak at 3506 cm⁻¹, which corresponds to the N–H stretch in lead(II)-halide-butylamine (PbX_n[NH(CH₂)CH₃]), shift to 3445 cm⁻¹. This shift associated with Mn²⁺ doping seems to be indicative of interaction between Mn and the N in the ligand as part of the MCs, in which Mn²⁺ replaced Pb²⁺.

The presence of $\mathrm{Mn^{2+}}$ within the MCs was further confirmed by EPR spectroscopy. As shown in Figure 5b, the EPR spectra of $\mathrm{Mn^{2+}}$ -doped MCs show a clear sextet hyperfine splitting pattern (hyperfine constant A = 88 G). Comparing the hyperfine splitting constant with the literature reports for Mn-doped perovskites, it is confirmed that Mn was present in the +2 oxidation state and resides in the size of Pb(II), experiencing an octahedral coordination environment around it. 37

The morphology of the host MCs and Mn^{2+} -doped MCs was determined using transmission electron microscopy (TEM). As shown in Figure 6, the average particle size for the undoped and Mn^{2+} -doped MCs is 0.9 ± 0.3 and 12 ± 3.3 nm, respectively. The Mn^{2+} -doped MCs seem to be agglomerated, likely because some $MnCl_2$ crystals are present. Previous studies of semiconductor clusters found that the clusters tend to grow or aggregate into larger into nanostructures upon drying. Thus, the measurement done on dried samples was likely for the larger or aggregated structures and not the original clusters in solution. Because of the

ultrasmall size of MCs, it is difficult to determine their size accurately.

On the basis of the above results, a model for the growth of Mn²⁺-doped MCs is proposed, as shown in Figure 7. MnCl₂ is used as Mn²⁺ precursor to dope MCs and produce Mn²⁺-doped MCs. With the addition of MnCl₂, the ion exchange reaction between Cl⁻ and Br⁻ occurs, as indicated by blue-shifted electronic absorption and PL spectra of the host MCs. Mn²⁺ doping only takes place at relatively high MnCl₂ concentration, as established on the basis of a combination of PL, PLE, TRPL, and EPR data. Interestingly, the Mn doping seems to be assisted by the Cl⁻ ion, in a codoping manner. At excessive Mn²⁺ concentrations, Mn—Mn coupling possibly occurred and resulted in a decrease or disappearance of Mn emission and a decrease in the PL lifetime.

In conclusion, we have demonstrated the successful synthesis of Mn²⁺-doped MCs by using OcAm or BTYA as capping ligand together with MnCl₂ as the Mn²⁺ doping source at room temperature. The incorporation of Mn²⁺dopants into the MCs was characterized using UV-vis, PLE, PL, TRPL, and EPR techniques. A blue shift of MCs electronic absorption and emission spectra is observed and attributed to the halogen ion exchange that occurs between Cl⁻ from MnCl₂ and Br⁻ in the MCs. Mn doping, replacing some Pb²⁺ ions, may be coupled with the Mn doping is evidenced by its characteristic emission peaked around 590 nm and PL lifetime of 1.28 ms as well as EPR data. This work demonstrates the first synthesis of Mn²⁺doped MCs that are potentially useful for single photon emission and other photonics applications. The strategy developed in the synthesis of Mn²⁺-doped MCs should be general and can be easily extended to other amine ligands.

EXPERIMENTAL METHODS

Materials. Lead bromide (PbBr₂, 99.0%, Aladdin), *n*-octylamine (OcAm, 99%, Aladdin), *n*-butylamine (BTYA, ≥ 99%, Aladdin), manganese chloride (MnCl₂, ≥ 99%, Aladdin),

manganese bromide (MnBr₂, 98%, Aladdin), N,N-dimethylformamide (DMF, \geq 99.9%, Ourchem), and toluene (\geq 99.8%, Ourchem) were commercially available. All chemicals were used as received without any further purification.

Synthesis of PbBr₂—OcAm. First, 0.080 mmol PbBr₂ was dissolved in 1.0 mL of DMF. Then 0.80 mmol OcAm was added and dissolved. Next, 100 μ L of the precursor solution was injected at a fast rate to 5.0 mL of toluene under vigorous stirring. Finally, 100 μ L of the as-synthesized solution was added to 5.0 mL of toluene for further characterization.

Synthesis of Mn^{2+} -Doped $PbBr_2$ -OcAm. Different amounts of MnX_2 (X = Cl or Br) were dissolved in 1.0 mL DMF. Then 100 μ L of the precursor solution was injected at a fast rate to 5.0 mL of the above as-synthesized $PbBr_2$ -OcAm solution under vigorous stirring. Finally, 100 μ L of the obtained solution was added to 5.0 mL of toluene to obtain Mn^{2+} -doped $PbBr_2$ -OcAm solution.

Synthesis of PbBr₂–BTYA. First, 0.080 mmol PbBr₂ was dissolved in 1.0 mL of DMF. Then 1.0 mmol BTYA was added and dissolved. Next, 100 μ L of the precursor solution was injected at a fast rate to 5.0 mL of toluene under vigorous stirring. Finally, 100 μ L of the as-synthesized solution was added to 5.0 mL of toluene for further characterization.

Synthesis of Mn^{2+} -Doped PbBr₂-BTYA. Different amounts of MnX₂ (X = Cl or Br) were dissolved in 1.0 mL of DMF. Then 100 μ L of the precursor solution was injected at a fast rate to 5.0 mL of the above as-synthesized PbBr₂-BTYA solution under vigorous stirring. Finally, 100 μ L of the obtained solution was added to 5.0 mL of toluene to obtain Mn²⁺-doped PbBr₂-BTYA solution.

Spectroscopic Measurements. The measurements were carried out directly in the original environment without purification. UV-vis absorption spectra were measured with a Hitachi U-3900 UV-vis spectrophotometer, and the photoluminescence (PL) spectra were measured using a F-7000 spectrofluorometer using a quartz cuvette (1.0 cm \times 1.0 cm) at room temperature. MCs PL lifetime (LT) measurements were performed on an Edinburgh Instruments Fluorescence Spectrometer FLS1000 with an EPLED-375 light source and a photomultiplier tube (900) detector. Mn²⁺ PL LT measurements were performed on an Edinburgh FLS1000 spectrometer with a 350 μ s lamp source. The infrared spectrum was recorded on a Fourier transform infrared (FT-IR) spectrophotometer (Thermo Scientific Nicolet 6700). The electron paramagnetic resonance (EPR) measurements were carried out with a Bruker EMXPLUS spectrometer. Transmission electron microscopy (TEM) was performed using a FEI Tecnai G2 F20 TEM microscope operated at 300 kV acceleration voltage. Inductively coupled plasma optical emission spectroscopy (ICP-OES) was implemented using a PerkinElmer 8300.

AUTHOR INFORMATION

Corresponding Authors

Jin Z. Zhang — Department of Chemistry and Biochemistry, University of California, Santa Cruz, California 95064, United States; orcid.org/0000-0003-3437-912X; Phone: +1-831-459-3776; Email: zhang@ucsc.edu Keliang Pan — Hubei Institute of Geosciences, Wuhan 430034, PR China; Email: pankeliang@hust.edu.cn

Authors

Li Liu — Research Institute of Agricultural Quality Standards and Testing Technology, Hubei Academy of Agricultural Science, Wuhan 430064, PR China; Department of Chemistry and Biochemistry, University of California, Santa Cruz, California 95064, United States

Ke Xu — Multiscale Crystal Materials Research Center, Shenzhen Institute of Advanced Technology, Chinese Academy of Sciences, Shenzhen 518055, PR China

Xitian Peng — Research Institute of Agricultural Quality Standards and Testing Technology, Hubei Academy of Agricultural Science, Wuhan 430064, PR China

Complete contact information is available at: https://pubs.acs.org/10.1021/acs.jpclett.1c02243

Notes

The authors declare no competing financial interest.

ACKNOWLEDGMENTS

This work is supported by the US NSF (CHE-1904547). L.L. is grateful for support from the Key Research and Development Program of Hubei Province of China (Grant No. 2020BBB078). We thank Dr. Binbin Luo for helpful discussions.

REFERENCES

- (1) Schulz, P.; Cahen, D.; Kahn, A. Halide Perovskites: Is It All about the Interfaces? *Chem. Rev.* **2019**, *119*, 3349–3417.
- (2) Quan, L. N.; Rand, B. P.; Friend, R. H.; Mhaisalkar, S. G.; Lee, T.-W.; Sargent, E. H. Perovskites for Next-Generation Optical Sources. *Chem. Rev.* **2019**, *119*, 7444–7477.
- (3) Lozano, G. The Role of Metal Halide Perovskites in Next-Generation Lighting Devices. *J. Phys. Chem. Lett.* **2018**, *9*, 3987–3997. (4) Tong, J.; Jiang, Q.; Zhang, F.; Kang, S. B.; Kim, D. H.; Zhu, K. Wide-Bandgap Metal Halide Perovskites for Tandem Solar Cells. *ACS Energy Lett.* **2021**, *6*, 232–248.
- (5) Zhang, Q.; Shang, Q.; Su, R.; Do, T. T. H.; Xiong, Q. Halide Perovskite Semiconductor Lasers: Materials, Cavity Design, and Low Threshold. *Nano Lett.* **2021**, *21*, 1903–1914.
- (6) Wei, Y.; Ma, T.; Chen, J.; Zhao, M.; Zeng, H. Metal Halide Perovskites for Optical Parametric Modulation. *J. Phys. Chem. Lett.* **2021**, *12*, 3090–3098.
- (7) Luo, B.; Naghadeh, S. B.; Zhang, J. Z. Lead Halide Perovskite Nanocrystals: Stability, Surface Passivation, and Structural Control. *Chem. Nano Mater.* **2017**, *3*, 456–465.
- (8) Liu, L.; Xu, K.; Vickers, E. T.; Allen, A. L.; Li, X.; Peng, L.; Zhang, J. Z. Varying the Concentration of Organic Acid and Amine Ligands Allows Tuning between Quantum Dots and Magic-Sized Clusters of CH₃NH₃PbBr₃ Perovskite: Implications for Photonics and Energy Conversion. ACS Appl. Nano Mater. 2020, 3, 12379–12387.
- (9) Vickers, E. T.; Chen, Z. Y.; Cherrette, V.; Smart, T.; Zhang, P.; Ping, Y.; Zhang, J. Z. Interplay between Perovskite Magic-Sized Clusters and Amino Lead Halide Molecular Clusters. *Research* **2021**, 2021, 6047971.
- (10) Pinkard, A.; Champsaur, A. M.; Roy, X. Molecular Clusters: Nanoscale Building Blocks for Solid-State Materials. *Acc. Chem. Res.* **2018**, *51*, 919–929.
- (11) Friedfeld, M. R.; Stein, J. L.; Ritchhart, A.; Cossairt, B. M. Conversion Reactions of Atomically Precise Semiconductor Clusters. *Acc. Chem. Res.* **2018**, *51*, 2803–2810.
- (12) Pun, A. B.; Mazzotti, S.; Mule, A. S.; Norris, D. J. Understanding Discrete Growth in Semiconductor Nanocrystals: Nanoplatelets and Magic-Sized Clusters. *Acc. Chem. Res.* **2021**, *54*, 1545–1554.
- (13) Hartley, C. L.; Kessler, M. L.; Dempsey, J. L. Molecular-Level Insight into Semiconductor Nanocrystal Surfaces. *J. Am. Chem. Soc.* **2021**, *143*, 1251–1266.
- (14) Mule, A. S.; Mazzotti, S.; Rossinelli, A. A.; Aellen, M.; Prins, P. T.; van der Bok, J. C.; Solari, S. F.; Glauser, Y. M.; Kumar, P. V.;

- Riedinger, A.; et al. Unraveling the Growth Mechanism of Magic-Sized Semiconductor Nanocrystals. *J. Am. Chem. Soc.* **2021**, *143*, 2037–2048.
- (15) Zhou, Y.; Chen, J.; Bakr, O. M.; Sun, H.-T. Metal-Doped Lead Halide Perovskites: Synthesis, Properties, and Optoelectronic Applications. *Chem. Mater.* **2018**, *30*, 6589–6613.
- (16) Pradhan, N. Mn-Doped Semiconductor Nanocrystals: 25 Years and Beyond. J. Phys. Chem. Lett. 2019, 10, 2574–2577.
- (17) Li, H. D.; Xu, Z. W.; Fu, Q. M.; Zhao, H. Y.; Ding, J. X.; Ma, Y. F.; Han, Y. B.; He, R.; Shi, L.; Wang, S. G.; et al. The role of Mn as dopant on the optoelectronic properties of MA(Pb_{1-x}Mn_x)Cl₃ single crystals. *Mater. Res. Express* **2019**, *6*, No. 086210.
- (18) Parobek, D.; Dong, Y.; Qiao, T.; Son, D. H. Direct Hot-Injection Synthesis of Mn-Doped CsPbBr₃ Nanocrystals. *Chem. Mater.* **2018**, 30, 2939–2944.
- (19) Cortecchia, D.; Mróz, W.; Neutzner, S.; Borzda, T.; Folpini, G.; Brescia, R.; Petrozza, A. Defect Engineering in 2D Perovskite by Mn(II) Doping for Light-Emitting Applications. *Chem.* **2019**, *5*, 2146–2158.
- (20) Zou, S. H.; Liu, Y. S.; Li, J. H.; Liu, C. P.; Feng, R.; Jiang, F. L.; Li, Y. X.; Song, J. Z.; Zeng, H. B.; Hong, M. C.; et al. Stabilizing Cesium Lead Halide Perovskite Lattice through Mn (II)-Substitution for Air-Stable Light-Emitting Diodes. *J. Am. Chem. Soc.* **2017**, *139*, 11443–11450.
- (21) Das Adhikari, S.; Guria, A. K.; Pradhan, N. Insights of Doping and the Photoluminescence Properties of Mn-Doped Perovskite Nanocrystals. *J. Phys. Chem. Lett.* **2019**, *10*, 2250–2257.
- (22) Xu, K.; Vickers, E. T.; Luo, B.; Allen, A. C.; Chen, E.; Roseman, G.; Wang, Q.; Kliger, D. S.; Millhauser, G. L.; Yang, W.; et al. First Synthesis of Mn-Doped Cesium Lead Bromide Perovskite Magic Sized Clusters at Room Temperature. *J. Phys. Chem. Lett.* **2020**, *11*, 1162–1169.
- (23) Liu, W.; Lin, Q.; Li, H.; Wu, K.; Robel, I.; Pietryga, J. M.; Klimov, V. I. Mn²⁺-Doped Lead Halide Perovskite Nanocrystals with Dual-Color Emission Controlled by Halide Content. *J. Am. Chem. Soc.* **2016**, *138*, 14954–14961.
- (24) Sheikh, T.; Nag, A. Mn Doping in Centimeter-Sized Layered 2D Butylammonium Lead Bromide (BA₂PbBr₄) Single Crystals and Their Optical Properties. *J. Phys. Chem. C* **2019**, *123*, 9420–9427.
- (25) Zhang, H.; Yao, J.; Fu, H. Ultrathin Monolayer Mn²⁺-Alloyed 2D Perovskite Colloidal Quantum Wells. *Adv. Opt. Mater.* **2021**, *9*, 2001135.
- (26) Dutta, S. K.; Dutta, A.; Das Adhikari, S.; Pradhan, N. Doping Mn²⁺ in Single-Crystalline Layered Perovskite Microcrystals. *ACS Energy Lett.* **2019**, *4*, 343–351.
- (27) Cheng, J.; Li, Y.; Qu, W.; Sun, M.; Liu, Y.; Shi, W.; Du, W.; Zhang, Y. Mechanochemical synthesis and characterization of Mndoped CsPbCl₃ perovskite nanocrystals. *J. Alloys Compd.* **2020**, 822, 153615.
- (28) Sihn, M. R.; Kirakosyan, A.; Jeon, M. G.; Choi, J. Suppressed Mn²⁺ doping in organometal halide perovskite nanocrystals by formation of two-dimensional (CH₃NH₃)₂MnCl₄. *Chem. Commun.* **2021**, *57*, 5055–5058.
- (29) Norman, T. J.; Magana, D.; Wilson, T.; Burns, C.; Zhang, J. Z.; Cao, D.; Bridges, F. Optical and Surface Structural Properties of Mn²⁺-Doped ZnSe Nanoparticles. *J. Phys. Chem. B* **2003**, *107*, 6309–6317.
- (30) Zhang, J. Z.; Cooper, J. K.; Gul, S. Rational Codoping as a Strategy to Improve Optical Properties of Doped Semiconductor Quantum Dots. *J. Phys. Chem. Lett.* **2014**, *5*, 3694–3700.
- (31) Cooper, J. K.; Gul, S.; Lindley, S. A.; Yano, J.; Zhang, J. Z. Tunable Photoluminescent Core/Shell Cu⁺-Doped ZnSe/ZnS Quantum Dots Codoped with Al³⁺, Ga³⁺, or In³⁺. ACS Appl. Mater. Interfaces **2015**, *7*, 10055–10066.
- (32) Gul, S.; Cooper, J. K.; Glans, P. A.; Guo, J. H.; Yachandra, V. K.; Yano, J. K.; Zhang, J. Z. Effect of Al³⁺ Co-doping on the DopantLocal Structure, Optical Properties, and Exciton Dynamics in Cu⁺-Doped ZnSe Nanocrystals. *ACS Nano* **2013**, *7*, 8680–8692.

- (33) Corrado, C.; Cooper, J. K.; Hawker, M.; Hensel, J.; Livingston, G.; Gul, S.; Vollbrecht, B.; Bridges, F.; Zhang, J. Z. Synthesis and Characterization of Organically Soluble Cu-Doped ZnS Nanocrystals with Br Co-activator. *J. Phys. Chem. C* **2011**, *115*, 14559–14570.
- (34) Huang, G.; Wang, C.; Xu, S.; Zong, S.; Lu, J.; Wang, Z.; Lu, C.; Cui, Y. Postsynthetic Doping of MnCl₂ Molecules into Preformed CsPbBr₃ Perovskite Nanocrystals via a Halide Exchange-Driven Cation Exchange. *Adv. Mater.* **2017**, *29*, 1700095.
- (35) Mir, W. J.; Jagadeeswararao, M.; Das, S.; Nag, A. Colloidal Mn-Doped Cesium Lead Halide Perovskite Nanoplatelets. *ACS Energy Lett.* **2017**, *2*, 537–543.
- (36) Liu, W.; Lin, Q.; Li, H.; Wu, K.; Robel, I.; Pietryga, J. M.; Klimov, V. I. Mn²⁺-Doped Lead Halide Perovskite Nanocrystals with Dual-Color Emission Controlled by Halide Content. *J. Am. Chem. Soc.* **2016**, *138*, 14954–14961.
- (37) Hills-Kimball, K.; Pérez, M. J.; Nagaoka, Y.; Cai, T.; Yang, H.; Davis, A. H.; Zheng, W.; Chen, O. Ligand Engineering for Mn²⁺ Doping Control in CsPbCl₃ Perovskite Nanocrystals via a Quasi-Solid-Solid Cation Exchange Reaction. *Chem. Mater.* **2020**, *32*, 2489–2500.
- (38) Yan, Z.; Li, N.; Wang, L.; Yu, Z.; Li, M.; Zhang, J.; Li, X.; Yang, K.; Gao, G.; Wang, L. Pressure-Induced Two-Color Photoluminescence and Phase Transition of Two-Dimensional Layered MnCl₂. *J. Phys. Chem. C* **2020**, *124*, 23317–23323.
- (39) Xu, K.; Allen, A. C.; Luo, B.; Vickers, E. T.; Wang, Q.; Hollingsworth, W. R.; Ayzner, A. L.; Li, X.; Zhang, J. Z. Tuning from Quantum Dots to Magic Sized Clusters of CsPbBr₃ Using Novel Planar Ligands Based on the Trivalent Nitrate Coordination Complex. J. Phys. Chem. Lett. 2019, 10, 4409–4416.